Research Article | Vol. 14, No. 10 / 1 Oct 2023 / Biomedical Optics Express 5085
Biomedical Optics EXPRESS

Two-photon imaging reveals histopathological changes in the gastric tumor microenvironment induced by neoadjuvant treatment

LIANHUANG LI,[1,5,†] SHICHAI HONG,[2,3,†] DEYONG KANG,[4] XINGXIN HUANG,[1] SHICHAO ZHANG,[1] ZHENLIN ZHANG,[1] YONGJIAN ZHOU,[2,6] AND JIANXIN CHEN[1]

[1]*Key Laboratory of OptoElectronic Science and Technology for Medicine of Ministry of Education, Fujian Provincial Key Laboratory of Photonics Technology, Fujian Normal University, Fuzhou 350007, China*
[2]*Department of Gastric Surgery, Fujian Medical University Union Hospital, Fuzhou 350001, China*
[3]*Department of Vascular Surgery, Zhongshan Hospital (Xiamen), Fudan University, Xiamen 361015, China*
[4]*Department of Pathology, Fujian Medical University Union Hospital, Fuzhou 350001, China*
[5]*lhli@fjnu.edu.cn*
[6]*zhouyjbju@163.com*
[†]These authors contributed equally to this work

Abstract: There is a close association between tumor response and survival in gastric cancer patients after receiving neoadjuvant treatment. An accurate and rapid assessment of therapeutic efficacy would be helpful for subsequent treatments and individual prognosis. At present, pathological examination is the gold standard for evaluating treatment response, however, it requires additional staining and the process is tedious, labor-intensive, as well as time-consuming. Here, we introduce a label-free imaging technique, two-photon imaging, to evaluate histopathological changes induced by pre-operative therapy, with a focus on assessing tumor regression as well as stromal response. Imaging data show that two-photon imaging allows label-free, rapid visualization of various aspects of pathological alterations in tumor microenvironment such as fibrotic reaction, inflammatory cell infiltration, mucinous response, isolated residual tumor cells. Moreover, a semi-automatic image processing approach is developed to extract the collagen morphological features, and statistical results show that there are significant differences in collagen area, length, width, cross-link space between the gastric cancer tissues with and without treatment. With the advent of a portable, miniaturized two-photon imaging device, we have enough reason to believe that this technique will become as an important auxiliary diagnostic tool in assessing neoadjuvant treatment response and thereby tailoring the most appropriate therapy strategies for the patients.

1. Introduction

Gastric cancer is a common malignant tumor of digestive tract, and the survival rate has been improved because of the implementation of a combined strategy of neoadjuvant treatment and surgery [1]. Clinical trials demonstrated that neoadjuvant treatment would improve overall and disease-free survival of patients with advanced gastric cancer [2,3]. Previous study revealed that perioperative chemotherapy has shown an improvement in 5-year overall survival compared to surgery alone (36% vs. 23%, respectively) [4]. Tumor response to the pre-operative therapy is considered to be a surrogate biomarker, allowing to predict prognosis and outcome of the disease. Most of patients will respond and even some patients may have pathologic complete response (pCR), but many patients do not respond. Therefore, there is a need to discriminate patients who will benefit from those who will not. Currently, post-operative histopathology could demonstrate high-resolution cellular morphology and tissue structures, and thereby serves as the

#501519 https://doi.org/10.1364/BOE.501519
Journal © 2023 Received 25 Jul 2023; revised 27 Aug 2023; accepted 1 Sep 2023; published 8 Sep 2023

Biomedical Optics EXPRESS

golden standard for treatment response. However, it is labor-intensive as well as time-consuming. Therefore, exploring a novel imaging technique with the ability to label-free image fresh tissue slice for pathological evaluation could be of great clinical utility.

Several optical imaging systems have been developed to label-free image biological tissues such as optical coherence tomography (OCT), photoacoustic microscopy (PAM), but they are not suitable for assessing histopathological changes due to limited resolution [5]. Two-photon microscopy, also termed multiphoton microscopy (MPM), has the potential to achieve this goal because it can provide optical images from biological tissues with high-resolution (comparable to pathological diagnosis) and without the need for exogenous contrast agents [6,7]. Many researchers have begun to assess two-photon imaging, a new non-destructive technology, that allows high-contrast imaging at a subcellular level and also permits repeated measurements of the same sample. For example, previous reports demonstrated that this technique is a powerful tool to study various kinds of malignant tumors, such as breast carcinoma, gastrointestinal cancers, hepatocellular carcinoma [8–10]. Moreover, multiphoton microscopy has been used for the analysis of cellular behavior that will contribute to our understanding of the priming and effector phases of immune responses [11]. Recently, two-photon imaging technique based on the combination of two-photon autofluorescence (TPAF) with second harmonic generation (SHG) imaging has been used to assess collagen morphological changes in tumor microenvironment [12] and neoadjuvant therapy responses in breast carcinoma [13]. These previous studies demonstrate that two-photon microscopy makes precise monitoring of histopathological changes possible, and thereby the present study is conducted to label-free assess the response of gastric cancer to neoadjuvant treatment by the implication of two-photon imaging.

2. Materials and methods

2.1. Sample preparation

The Institutional Review Board of Fujian Medical University Union Hospital approved this research, and all patients provided written informed consent before study participation. Patients undergoing neoadjuvant treatment received either 2 or 4 preoperative cycles of SOX regimen (Tegafur Gimeracil Oteracil Potassium Capsule (S-1) plus Oxaliplatin) every 3 weeks, and antitumor efficacy was evaluated by CT scan after every two cycles. 45 cases of fresh gastric samples were taken from patients undergoing surgical resection, including 15 normal tissues, 15 tumors with neoadjuvant treatment and 15 tumors without treatment. Two serial sections (10μm) were cut from each sample by a cryostat microtome, and thereinto, a fresh section was used for two-photon imaging and an adjacent section was stained with hematoxyline and eosin (H&E). All the digital images of H&E-stained slices were acquired via a whole slide scanner (VM1000, Motic, China), and were processed with the Motic DSAssistant Lite software. Two-photon images were then compared with the corresponding H&E-stained images (prepared from the adjacent sections) to confirm experimental results.

2.2. Two-photon imaging system

The imaging system mainly composes of two parts: a laser scanning confocal microscope (LSM 880, Zeiss, Germany) and a mode-locked femtosecond Ti: sapphire laser (Chameleon Ultra, Coherent, USA), tunable from 690 nm to 1064 nm. In this work, tissue sections were excited using linearly polarized 810 nm laser (110 fs, 76 MHz) and were observed using a Plan-Apochromat oil immersion objective (63×, NA 1.4, Zeiss) in multi-track channel mode. SHG signal (color-coded with green) was collected between 394 and 416 nm in one channel via a GaAsP photomultiplier tube (PMT), and meantime TPAF signal (color-coded with red) was detected between 430 and 759 nm in another channel by a 32-channel GaAsP PMT array. For this system, a lateral resolution of 0.3 μm as well as an axial resolution of 0.8 μm could be achieved, and it takes 1.8 μs for

Biomedical Optics EXPRESS

collecting each pixel. All images had a 12-bit pixel depth in our experiment, and large-area images were obtained by automatically assembling an array of images with 512×512 pixels (field of view, FOV) using ZEN imaging software.

2.3. Statistical analysis

Statistical analysis was performed by the IBM SPSS Statistics 21. The two-sample t-test (also called independent samples t-test) was conducted to assess statistical significance, and $P \leq 0.05$ was considered to be statistically significant.

3. Results

3.1. Two-photon imaging of normal and abnormal gastric tissues

Neoadjuvant treatment is a standard of care for patients with advanced gastric cancer, in which tumor has penetrated into the muscular layer or beyond. Therefore, in this work, our interest mainly focuses on gastric muscularis. For the sake of comparison, we first performed two-photon imaging on the normal gastric tissues. As shown in Fig. 1, this imaging technique has the ability to provide detailed microstructural features of muscle tissues, where collagen fibers can emit SHG signal and elastin can generate TPAF signal. Sparse collagen fibers result in a relatively weak SHG signal (Fig. 1(A), (E)), by contrast, TPAF signal is strong owing to abundant elastin (Fig. 1(B)). Additionally, combining SHG with TPAF imaging enables us to understand the spatial distribution patterns of tissue components (Fig. 1(C), (F)), which may be helpful to accurately monitor microenvironmental changes in biological tissues. The next step is to assess whether a combination of TPAF and SHG imaging could be useful to detect the abnormal configurations of stomach.

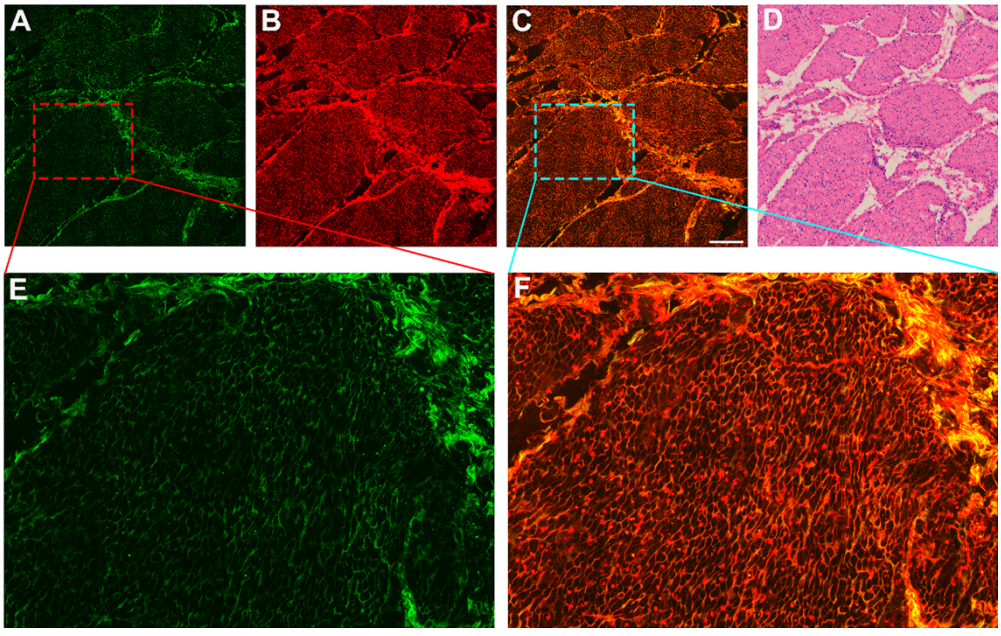

Fig. 1. Two-photon imaging of normal gastric muscularis and a corresponding H&E-stained image. Scale bar = 200μm. Pseudo-color presentation in the two-photon images: green—SHG; red—TPAF. (A) SHG image; (B) TPAF image; (C) Composite image (SHG + TPAF); (D) H&E-stained image; and (E-F) Magnified images of the regions of interest (red and cyan dashed boxes, respectively).

Biomedical Optics EXPRESS

Generally, the histopathological appearance of tumor would become complicated and confusing comparing to normal tissues. As displayed in Fig. 2, two-photon images of muscular layer with an infiltrating adenocarcinoma compose of many nest-like tumors cells, collagen fibers, and broken muscular tissues. The muscularis (cyan arrows in Fig. 2(B)) is degrading with tumor invasion and is replacing by many malignant cell clusters with gland-like structure (white arrows in Fig. 2(E)). These malignant glands often are surrounded by collagen fibers (pink arrows in Fig. 2(D)). Another significant change is obvious collagen accumulation, termed desmoplastic reaction, by comparing with normal muscularis (Fig. 1). SHG image shows that collagen fibers increase remarkably, and collagen network from abnormal muscularis (Fig. 2(A), (D)) becomes more confusing than that from normal tissues (Fig. 1(A), (E)).

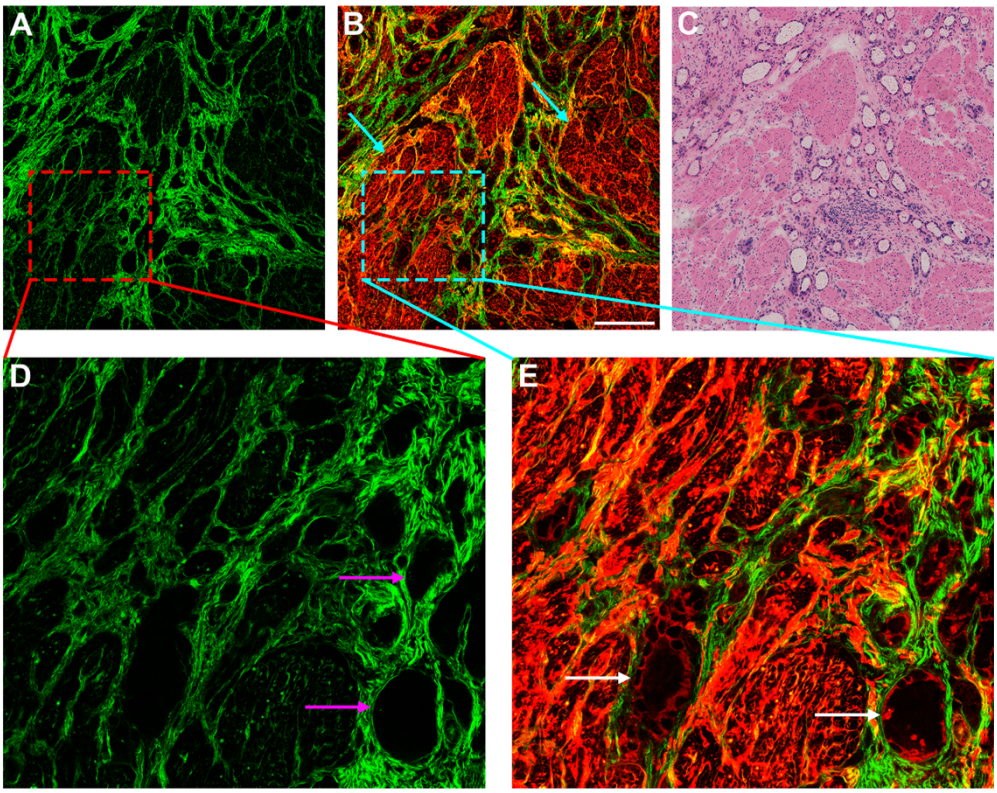

Fig. 2. Two-photon imaging of gastric muscularis with tumor invasion as well as severe desmoplastic reaction and a corresponding H&E-stained image. Scale bar = 200μm. Pseudo-color presentation in the two-photon images: green—SHG; red—TPAF. (A) SHG image; (B) Composite image (SHG + TPAF); (C) H&E-stained image; and (D-E) Magnified images of the regions of interest (red and cyan dashed boxes, respectively). Cyan arrows: broken muscular tissues; pink arrows: collagen fibers surrounding tumors; white arrows: adenocarcinoma with nest-like pattern.

Two-photon images presented in Fig. 3 demonstrates that tumors have infiltrated beyond the muscular layer and invaded into the serosal layer. The serosa, which acts as a barrier for the stomach from other organs, is characterized by lots of collagenous fibers (below the dashed red line in Fig. 3(A)) via SHG imaging. Remaining muscle tissues (cyan arrows in Fig. 3(B)) and nest-like tumors (white arrows in Fig. 3(E)) are also present by the combination of TPAF imaging. Interestingly enough, imaging results reveal that nerve fibers would emit strong TPAF signal, and thereby myenteric nerve plexuses (blue arrows in Fig. 3(D)) are detected too. These

Biomedical Optics EXPRESS

nervous fibers are dense and show wavy structures. Overall, it is obvious that multiplexing SHG with TPAF imaging techniques enables us to precisely detect the microstructural changes in tumor microenvironment, for instance, tumor infiltration, tumor boundary, desmoplastic response, perineural invasion, and so on.

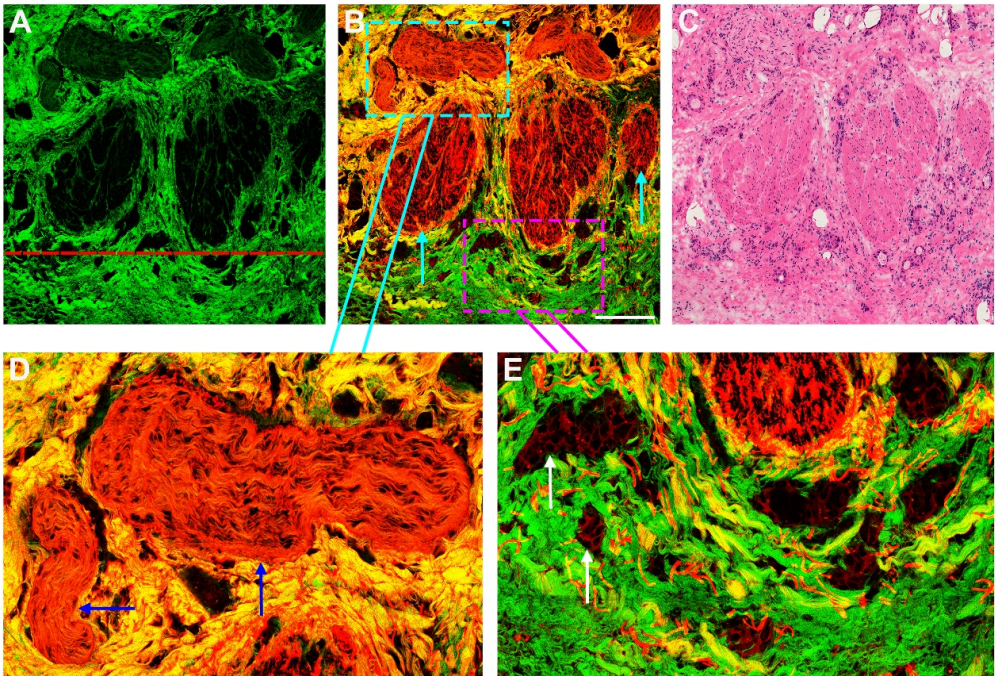

Fig. 3. Two-photon imaging of gastric serosa with tumor invasion and a corresponding H&E-stained image. Scale bar = 200μm. Pseudo-color presentation in the two-photon images: green—SHG; red—TPAF. (A) SHG image; (B) Composite image (SHG + TPAF); (C) H&E-stained image; and (D-E) Magnified images of the regions of interest (cyan and pink dashed boxes, respectively). Cyan arrows: remaining muscular tissues; blue arrows: myenteric nerve plexus; white arrows: tumor cells with nest-like structure.

3.2. Assessing neoadjuvant treatment responses by two-photon imaging

The histopathologic appearance of tumors after pre-operative treatment would change significantly, and even changes in tumor morphology can occur before the alteration in tumor size and may accompany disease regression. Therefore, in this part, post-therapy gastric cancer tissues are evaluated for morphologic changes via two-photon imaging. Figure 4 displays two-photon images of tumor response to neoadjuvant treatment and a corresponding H&E-stained image. Compared with the SHG image of normal muscularis (Fig. 1(A)), there is clear fibrotic change (Fig. 4(A), (D)) in muscular layer caused by pre-operative treatment. By combining with TPAF imaging, we can further find that tumor regression appears, residual gland-like tumor (white arrow in Fig. 4(E)) is collapsing, and there is a small amount of remaining muscle tissue (blue arrow in Fig. 4(B)). Tumor cells may be sparse and isolated after treatment, and therefore can easily be neglected. However, our experimental results reveal that two-photon microscopy is able to visualize residual tumor cells without the use of exogenous contrast agents.

Drug-induced morphologic changes in stroma mainly consist of fibrosis, mucinous response, inflammatory reaction, blood vessel hyperplasia, and so on [14]. As shown in Fig. 5, mucinous response is well presented by two-photon images, where SHG imaging shows that collagen

Biomedical Optics EXPRESS

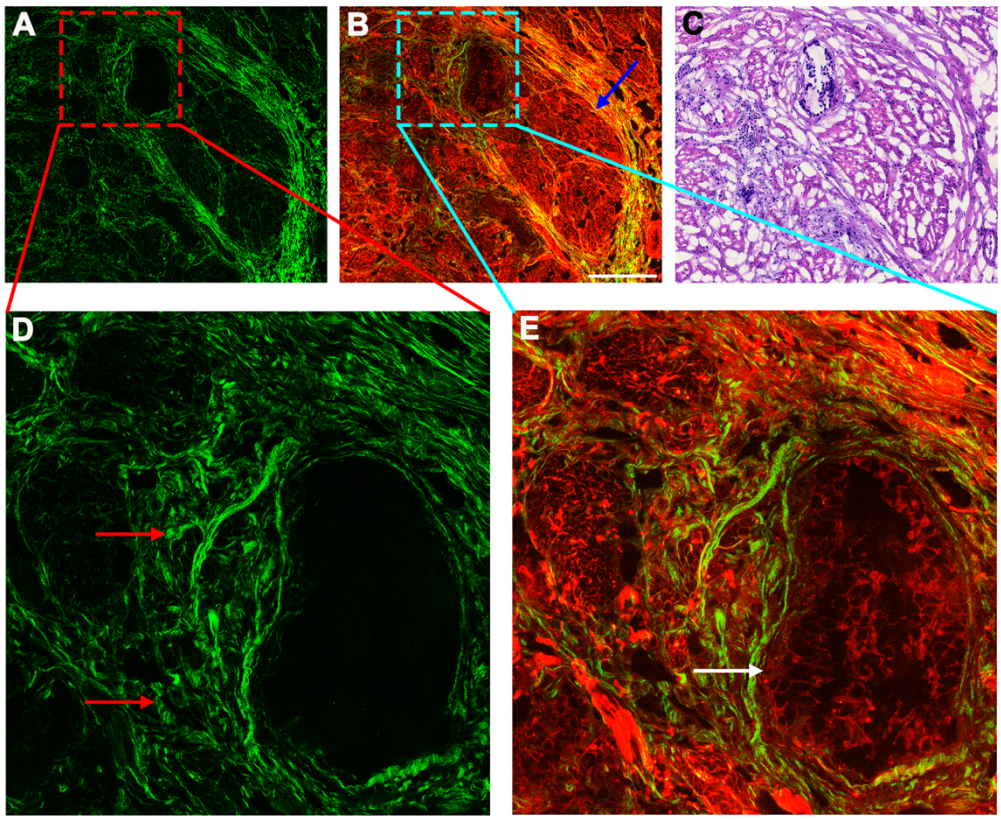

Fig. 4. Two-photon imaging of tumor response to neoadjuvant treatment and a corresponding H&E-stained image. Scale bar = 200μm. Pseudo-color presentation in the two-photon images: green—SHG; red—TPAF. (A) SHG image; (B) Composite image (SHG + TPAF); (C) H&E-stained image; and (D-E) Magnified images of the regions of interest (red and cyan dashed boxes, respectively). Blue arrow: residual muscle tissue; red arrows: fibrosis change; white arrow: remaining tumor.

fibers are very sparse (Fig. 5(A)), but TPAF imaging reveals that there are many residual tumor cells (cyan arrows in Fig. 5(D)) floating in mucin pool, large areas of cellular necrosis (yellow arrows in Fig. 5(D)), as well as some abnormal elastic fibers (white arrows in Fig. 5(E)). These pathologic alterations are difficult to identify via H&E-stained image because they are covered by mucin pool (Fig. 5(C)), however, can be easily detected by two-photon imaging as stromal mucin does not emit multiphoton signals. In addition, some residual malignant glands (blue arrow in Fig. 5(E)) that are decomposing but still retain gland-like structure are also found by TPAF imaging.

Inflammatory response often begins early in the therapeutic process and becomes persistent through life in most patients. Figure 6 displays two-photon images of inflammatory response accompanying with obvious fibrosis. Fibrotic reaction (pink arrows in Fig. 6(A)) reflects the self-healing capability of biological tissues after tumor regression. When incorporating with TPAF imaging, we can find severe inflammatory infiltration (Fig. 6(B)) that is in excellent agreement with H&E-stained image (Fig. 6(C)). Large numbers of lymphocytes with a small and round nucleus (white arrows in Fig. 6(E)) have infiltrated into the stroma, and some reticular fibers (Fig. 6(D)), which are around the inflammatory cells and may be used to support these cells, are detected too.

Biomedical Optics EXPRESS

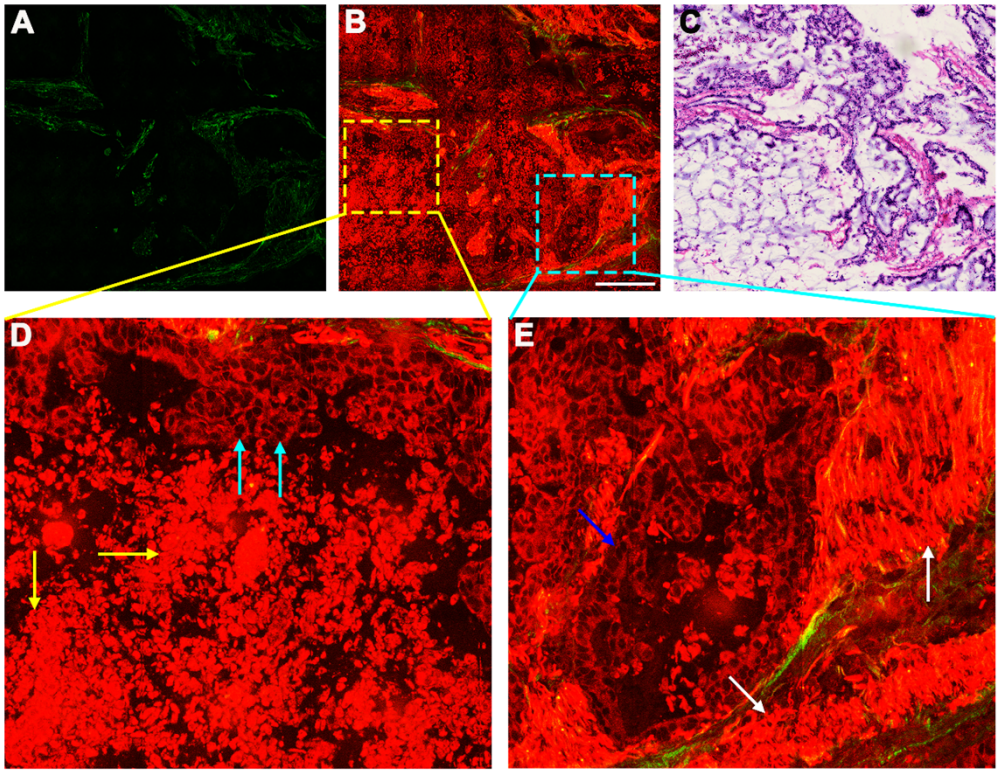

Fig. 5. Two-photon imaging of mucinous response caused by neoadjuvant treatment and a corresponding H&E-stained image. Scale bar = 200μm. Pseudo-color presentation in the two-photon images: green—SHG; red—TPAF. (A) SHG image; (B) Composite image (SHG + TPAF); (C) H&E-stained image; and (D-E) Magnified images of the regions of interest (yellow and cyan dashed boxes, respectively). Yellow arrows: tumor necrosis; cyan arrows: tumor cells floating in mucin pool; blue arrow: tumor cells with gland-like cluster; white arrows: abnormal elastic fibers that are short and thick in shape as well as flock together.

It is important to point out that neoadjuvant treatment affects not only the tumors, but also the surrounding healthy tissues. Therefore, we also observe the adjacent normal muscularis using two-photon microscopy. The most significant effect is to cause collagen deposition. As shown in Fig. 7(A), there are obvious fibrosis changes in the adjacent muscle tissues. The muscular layer becomes rich in collagenous fibers by comparing with the normal muscularis without pre-operative treatment (Fig. 1(A)). These fibers (red arrows in Fig. 7(D)) are thick, short as well as chaotic. In addition, composite images (Fig. 7(B), (E)) could present the relative spatial distributions of tissue components well. It is well-known that the resultant degree of fibrosis after neoadjuvant therapy may radiologically mimic malignant tissues. Our imaging data reveal that fibrotic changes can be accurately identified via SHG imaging.

3.3. Quantitative analysis on SHG images

In this section, we further performed imaging analysis on SHG images to analyze the collagen morphological difference between gastric cancer samples from patients with and without receiving pre-operative treatment. To quantitatively monitor collagen changes in tumor microenvironment, we developed an automatic image processing method, as previously described [15], for quantifying

Biomedical Optics EXPRESS

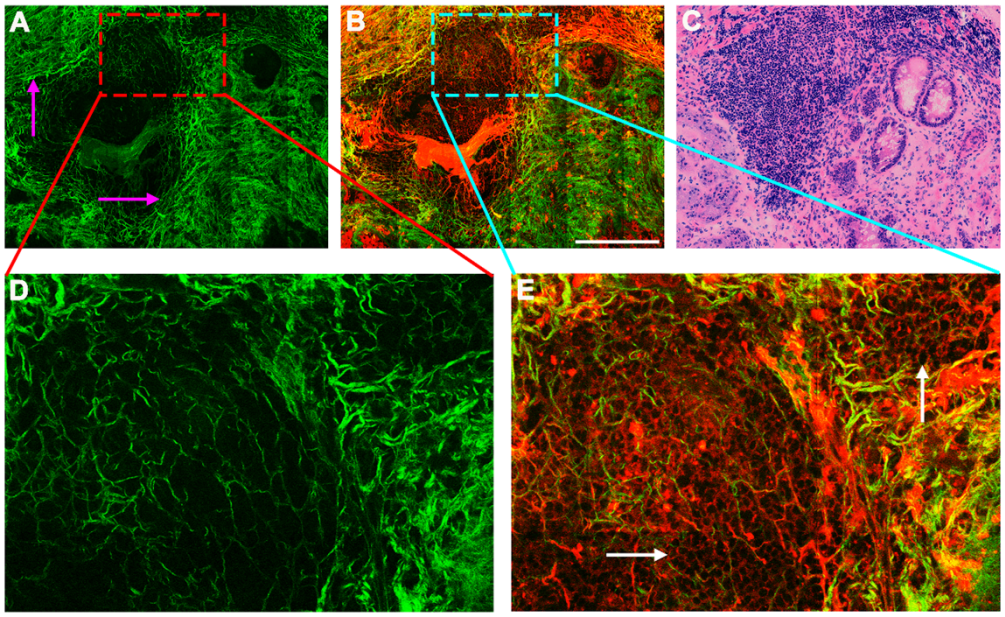

Fig. 6. Two-photon imaging of inflammatory response induced by neoadjuvant treatment and a corresponding H&E-stained image. Scale bar = 200μm. Pseudo-color presentation in the two-photon images: green—SHG; red—TPAF. (A) SHG image; (B) Composite image (SHG + TPAF); (C) H&E-stained image; and (D-E) Magnified images of the regions of interest (red and cyan dashed boxes, respectively). Pink arrows: significant fibrotic response; white arrows: lymphocytes.

morphology characterization on SHG images, including collagen proportionate area (a.u.), number (per mm^2), length (μm), width (μm), straightness (a.u.), cross-link density (a.u.), cross-link space (μm), and orientation (a.u.). The collagen proportionate area is the percentage of pixels belonging to collagen fibers in the segmented image, collagen number is defined as the number of extracted fibers per mm^2, collagen length, width, straightness, and cross-link space are regarded as the mean length, width, straightness, and cross-link space of the identified collagen fibers respectively, collagen cross-link density is defined as the ratio of the total number of cross-link points to the sum of lengths of all collagen fibers, and collagen orientation is the main orientation identified from the angular orientation distribution of the Fourier transformed image. At present, neoadjuvant therapy is a standard treatment for locally advanced gastric cancer, indicating tumor cells have spread through the submucosa, and thereby our interest is focused on the muscular layer. For a total of 30 tumor samples including 15 samples with therapy and 15 samples without therapy, 25 regions of interest (ROIs) with the size of 512×512 pixels (135μm×135 μm) were randomly chosen from each sample for quantitative analysis.

Quantitative results are presented using means with standard deviations (SDs) as shown in Table 1, thereinto, no differences ($P > 0.05$) are found in the collagen number, straightness, cross-link density as well as orientation, but significant differences ($P < 0.05$) are found in the proportionate area, length, width, and cross-link space of collagen fibers when comparing cancer tissues with treatment and those without, demonstrating neoadjuvant treatment would induce some morphological alterations of collagen fibers. These results indicate that it is possible to qualitatively and quantitatively monitor the collagenous variations in tumor microenvironment before and after treatment without the use of exogenous contrast agents by the combination of two-photon imaging with imaging analysis.

Biomedical Optics EXPRESS

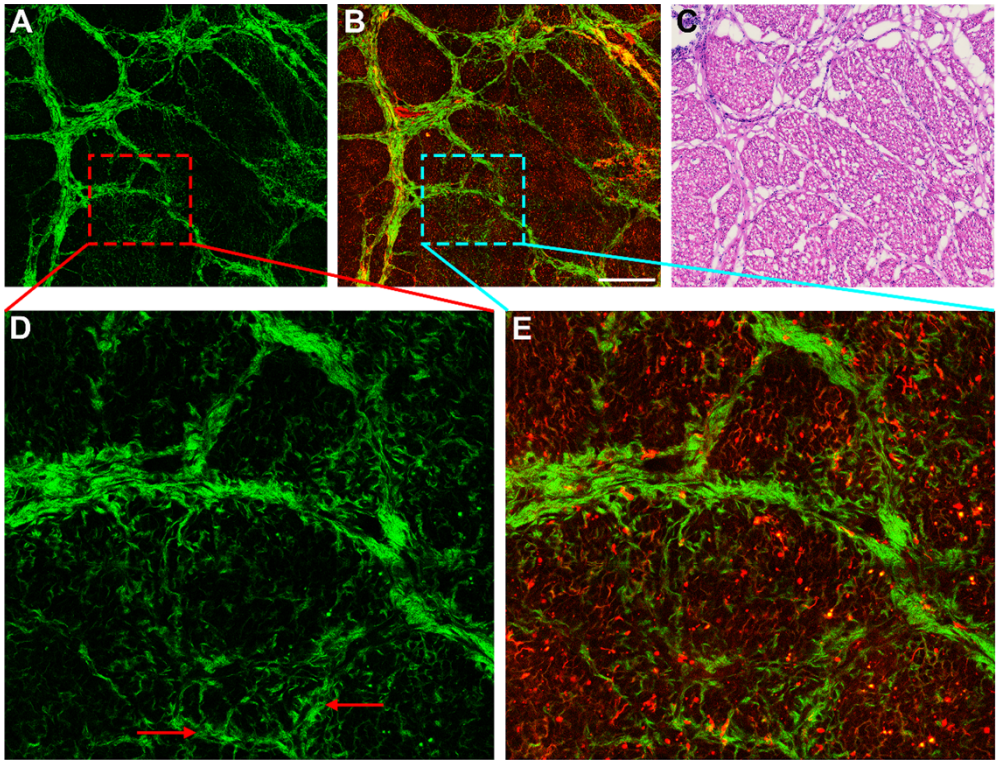

Fig. 7. Two-photon imaging of fibrotic changes in adjacent normal muscularis caused by neoadjuvant treatment and a corresponding H&E-stained image. Scale bar = 200μm. Pseudo-color presentation in the two-photon images: green—SHG; red—TPAF. (A) SHG image; (B) Composite image (SHG + TPAF); (C) H&E-stained image; and (D-E) Magnified images of the regions of interest (red and cyan dashed boxes, respectively). Red arrows: collagen hyperplasia in muscle tissues.

Table 1. A comparison of collagen features from the gastric cancer tissues with and without treatment

Quantitative parameters	Samples		
	Without treatment	With treatment	*P*-value
Area	0.2495 ± 0.1226	0.2833 ± 0.1506	0.0022
Number	0.0118 ± 0.0050	0.0127 ± 0.0058	0.0706
Length	11.1332 ± 1.8869	11.4397 ± 2.5577	<0.0001
Width	1.3441 ± 0.3629	1.5185 ± 0.4749	<0.0001
Straightness	0.9300 ± 0.0100	0.9318 ± 0.0112	0.2519
Cross-link density	0.0123 ± 0.0019	0.0116 ± 0.0021	0.0702
Cross-link space	31.0767 ± 5.1190	32.6132 ± 6.4005	<0.0001
Orientation	0.6261 ± 0.2005	0.7013 ± 0.1890	0.3542

Biomedical Optics EXPRESS

4. Discussion

Gastric cancer is one of the most common malignant tumors in the world, and is a leading cause of cancer-related death due to its aggressive biological behavior [16]. Surgery alone is not sufficient treatment [4], and now neoadjuvant treatment has been accepted as the standard-of-care for locally-advanced gastric cancer with the goals of increasing the rates of curative surgical resection and improving survival [17,18]. Assessing the response of gastric tumor to pre-operative therapy after surgery can provide prognostic information to help guide follow up care. Above all, it is crucial to determine responders versus non-responders in order to help guide treatment decisions. In patients who will not respond sufficiently, costly but ineffective neoadjuvant chemotherapy should not be continued or, preferably, even not be started. The evaluation of pathological response after treatment based on clinical examination techniques such as endoscopic ultrasonography (EUS), computerized tomography (CT), is still not satisfactory at present [19]. Histopathological diagnosis of post-operative samples remains the gold standard for evaluating therapeutic efficacy, however, it needs additional staining and is tedious, labor-intensive, as well as time-consuming. Therefore, the need for label-free observation of cells and other tissue components in biological tissues is of great interest and imaging techniques have been developed to pursue this goal.

Two-photon microscopy has the ability to label-free assess a tissue section in minutes, without needing to wait for tissue processing and staining [20,21], and this might help improve diagnostic turnaround time, especially in time-sensitive contexts. This imaging technique has been widely used for microscopic examination in gastrointestinal tract to distinguish healthy from diseased tissues, for example, Cicchi et al. utilized MPM to observe morphological alterations in colon mucosa to discriminate adenomatous polyp and adenocarcinoma from normal tissues [22], Rogart et al. used multiphoton imaging for the examination of intact human gastrointestinal mucosa ex vivo [23], and we employed two-photon imaging to identify premalignant gastric lesions including intestinal metaplasia as well as intraepithelial neoplasia [24]. These previous results demonstrate that two-photon imaging permits instant visualization of histopathological alterations in tumors following neoadjuvant therapy.

Our imaging results prove that two-photon microscopy is capable of label-free detecting pathological changes caused by neoadjuvant treatment, such as tumor regression, fibrosis, mucinous response, inflammatory cell infiltration, and so on. Histopathologic tumor regression to pre-operative therapy is considered to be a prognostic marker for long-term survival in gastric carcinoma. TPAF imaging is suitable for detecting residual tumors (shown in Fig. 4), and even single tumor cell (shown in Fig. 5) because of the endogenous fluorescent molecules in cells such as FAD, NADH [25,26]. Generally speaking, tumor invasion would cause an excessive collagen fibers, termed desmoplastic reaction (shown in Fig. 2), and tumor regression often accompanies with remarkable increase of collagen content, called stromal fibrosis (shown in Fig. 4). Desmoplastic reaction reflects the self-protection of tumors, while stromal fibrosis is an indicator of the self-repairing capability of tissues. SHG imaging is able to discern these pathological variations since collagen fibers form a non-centrosymmetric structure and thus could emit strong SHG signal [27]. Interestingly, two-photon imaging also reveals that neoadjuvant treatment would induce fibrotic changes in adjacent normal tissues (shown in Fig. 7(A)).

It is well-known that collagen morphology in tumor microenvironment will change significantly during tumor development, and some quantification methods beyond collagen alignment, such as tumor-associated collagen signature (TACS) [12,28] and aspect ratio (AR) [29], have been used to provide quantitative information. We also conducted a series of image analyses to quantitatively evaluate the collagen morphological difference in cancerous tissues with and without treatment. Statistical analyses show that there are obvious differences in collagen proportionate area, length, width, and cross-link space, and quantitative results of the four features from the treated cancer tissues are larger than that from the cancerous tissues without treatment,

Biomedical Optics EXPRESS

indicating fibrotic changes appear after tumor regression, and these collagen fibers are longer and thicker. These features may be treated as optical biomarkers to help monitor collagen changes in tumor microenvironment through the combination of two-photon imaging with image analysis. Recently, Sun et al. have successfully developed a compact and portable multiphoton imaging system integrating four nonlinear optical imaging modalities for the intraoperative visualization of tumor microenvironment [8], and Kreiß et al. reported that they have used multiphoton endomicroscopy to achieve label-free, in vivo histopathology of experimental colitis in animals [30]. Hence, we firmly believe that this imaging technology may open new avenues for immediate assessment of tumor response following neoadjuvant treatment. It should be noted that this study has some limitations: firstly, the sample size is small; secondly, quantitative analysis cannot be carried out automatically by deep learning or other techniques. Maybe, our future work should focus on the combination of multiphoton imaging with machine learning to obtain more comprehensive information quickly and objectively. Additionally, it needs to develop a fast, portable, and compact label-free imaging system that could integrate multimodal nonlinear optical imaging such as TPAF, SHG to realize clinical utility.

5. Conclusion

In summary, two-photon microscopy successfully visualizes the pathological changes in gastric tumor microenvironment induced by neoadjuvant therapy, and therefore could be used for label-free assessing therapeutic effects by monitoring tumor regression and identifying various kinds of stromal response. Besides, with the aid of imaging processing technique, collagen morphological features are quantitatively analyzed and significant differences are found between the cancerous tissues with and without treatment in collagen fiber area, length, width, cross-link space. With the continue advancement of multiphoton imaging technique, it can be predicted that this technology may play an important role in evaluating tumor response and informing clinical decisions in the neoadjuvant setting.

Funding. National Natural Science Foundation of China (82171991, 82172800); Natural Science Foundation of Fujian Province (2023J01082); Joint Funds for the Innovation of Science and Technology of Fujian Province (2019Y9101).

Disclosures. The authors declare that they have no competing interests.

Data availability. The datasets used and/or analyzed during the study are available from the corresponding author on reasonable request.

References

1. C. Kaltenmeier, A. Althans, M. Mascara, I. Nassour, S. Khan, R. Hoehn, A. Zureikat, and S. Tohme, "Pathologic complete response following neoadjuvant therapy for gastric adenocarcinoma: a national cancer database analysis on incidence, predictors, and outcomes," Am. Surg. **87**(7), 1145–1154 (2021).
2. N. Ikoma, J. S. Estrella, M. Blum Murphy, P. Das, B. D. Minsky, P. Mansfield, J. A. Ajani, and B. D. Badgwell, "Tumor Regression Grade in Gastric Cancer After Preoperative Therapy," Journal of Gastrointestinal Surgery **25**(6), 1380–1387 (2021).
3. T. Yoshikawa, Y. Rino, N. Yukawa, T. Oshima, A. Tsuburaya, and M. Masuda, "Neoadjuvant chemotherapy for gastric cancer in Japan: a standing position by comparing with adjuvant chemotherapy," Surg. Today **44**(1), 11–21 (2014).
4. D. Cunningham, W. H. Allum, S. P. Stenning, J. N. Thompson, C. J. Van de Velde, M. Nicolson, J. H. Scarffe, F. J. Lofts, S. J. Falk, T. J. Iveson, D. B. Smith, R. E. Langley, M. Verma, S. Weeden, Y. J. Chua, and M. T. Participants, "Perioperative chemotherapy versus surgery alone for resectable gastroesophageal cancer," N. Engl. J. Med. **355**(1), 11–20 (2006).
5. R. Weissleder and M. J. Pittet, "Imaging in the era of molecular oncology," Nature **452**(7187), 580–589 (2008).
6. T. Matsui, R. Tamoto, A. Iwasa, M. Mimura, S. Taniguchi, T. Hasegawa, T. Sudo, H. Mizuno, J. Kikuta, I. Onoyama, K. Okugawa, M. Shiomi, S. Matsuzaki, E. Morii, T. Kimura, K. Kato, Y. Kiyota, and M. Ishii, "Nonlinear optics with near-infrared excitation enable real-time quantitative diagnosis of human cervical cancers," Cancer Res. **80**(17), 3745–3754 (2020).
7. Y. Li, B. Shen, G. Zou, R. Hu, Y. Pan, J. Qu, and L. Liu, "Super-multiplex nonlinear optical imaging unscrambles the statistical complexity of cancer subtypes and tumor microenvironment," Adv. Sci. **9**, e2104379 (2022).
8. Y. Sun, S. You, H. Tu, D. R. Spillman Jr., E. J. Chaney, M. Marjanovic, J. Li, R. Barkalifa, J. Wang, A. M. Higham, N. N. Luckey, K. A. Cradock, Z. George Liu, and S. A. Boppart, "Intraoperative visualization of the tumor

Biomedical Optics EXPRESS

microenvironment and quantification of extracellular vesicles by label-free nonlinear imaging," Sci. Adv. **4**(12), eaau5603 (2018).
9. D. Chen, Z. Liu, W. Liu, M. Fu, W. Jiang, S. Xu, G. Wang, F. Chen, J. Lu, H. Chen, X. Dong, G. Li, G. Chen, S. Zhuo, and J. Yan, "Predicting postoperative peritoneal metastasis in gastric cancer with serosal invasion using a collagen nomogram," Nat. Commun. **12**(1), 179 (2021).
10. Y. Wang, G. L. Wong, F. P. He, J. Sun, A. W. Chan, J. Yang, S. S. Shu, X. Liang, Y. K. Tse, X. T. Fan, J. Hou, H. L. Chan, and V. W. Wong, "Quantifying and monitoring fibrosis in non-alcoholic fatty liver disease using dual-photon microscopy," Gut **69**(6), 1116–1126 (2020).
11. D. Schienstock and S. N. Mueller, "Moving beyond velocity: opportunities and challenges to quantify immune cell behavior," Immunological Reviews **306**(1), 123–136 (2022).
12. G. Xi, W. Guo, D. Kang, J. Ma, F. Fu, L. Qiu, L. Zheng, J. He, N. Fang, J. Chen, J. Li, S. Zhuo, X. Liao, H. Tu, L. Li, Q. Zhang, C. Wang, S. A. Boppart, and J. Chen, "Large-scale tumor-associated collagen signatures identify high-risk breast cancer patients," Theranostics **11**(7), 3229–3243 (2021).
13. L. Li, Z. Han, L. Qiu, D. Kang, Z. Zhan, H. Tu, and J. Chen, "Label-free multiphoton imaging to assess neoadjuvant therapy responses in breast carcinoma," Int. J. Biol. Sci. **16**(8), 1376–1387 (2020).
14. K. Becker, J. D. Mueller, C. Schulmacher, K. Ott, U. Fink, R. Busch, K. Böttcher, J. R. Siewert, and H. Höfler, "Histomorphology and grading of regression in gastric carcinoma treated with neoadjuvant chemotherapy," Cancer **98**(7), 1521–1530 (2003).
15. G. Xi, L. Qiu, S. Xu, W. Guo, F. Fu, D. Kang, L. Zheng, J. He, Q. Zhang, L. Li, C. Wang, and J. Chen, "Computer-assisted quantification of tumor-associated collagen signatures to improve the prognosis prediction of breast cancer," BMC Med. **19**(1), 273 (2021).
16. H. Sung, J. Ferlay, R. L. Siegel, M. Laversanne, I. Soerjomataram, A. Jemal, and F. Bray, "Global cancer statistics 2020: GLOBOCAN estimates of incidence and mortality worldwide for 36 cancers in 185 countries," Ca-Cancer J. Clin. **71**, 209–249 (2021).
17. A. Rajabnejad, F. Vaida, M. Valasek, S. Razzaque, P. Fanta, S. Horgan, M. Bouvet, A. M. Lowy, and K. J. Kelly, "Predictors and significance of histologic response to neoadjuvant therapy for gastric cancer," J. Surg. Oncol. **123**(8), 1716–1723 (2021).
18. J. H. Yeh, Y. S. Yeh, H. L. Tsai, C. W. Huang, T. K. Chang, W. C. Su, and J. Y. Wang, "Neoadjuvant Chemoradiotherapy for Locally Advanced Gastric Cancer: Where Are We at?" Cancers **14**(12), 3026 (2022).
19. R. M. Kwee and T. C. Kwee, "Role of imaging in predicting response to neoadjuvant chemotherapy in gastric cancer," World J. Gastroenterol. **20**(7), 1650–1656 (2014).
20. S. A. Boppart, S. You, L. Li, J. Chen, and H. Tu, "Simultaneous label-free autofluorescence-multiharmonic microscopy and beyond," APL Photonics **4**(10), 100901 (2019).
21. A. Dilipkumar, A. Al-Shemmary, L. Kreiss, K. Cvecek, B. Carle, F. Knieling, J. Gonzales Menezes, O. M. Thoma, M. Schmidt, M. F. Neurath, M. Waldner, O. Friedrich, and S. Schurmann, "Label-free multiphoton endomicroscopy for minimally invasive in vivo imaging," Adv. Sci. **6**(8), 1801735 (2019).
22. R. Cicchi, A. Sturiale, G. Nesi, D. Kapsokalyvas, G. Alemanno, F. Tonelli, and F. S. Pavone, "Multiphoton morpho-functional imaging of healthy colon mucosa, adenomatous polyp and adenocarcinoma," Biomed. Opt. Express **4**(7), 1204–1213 (2013).
23. J. N. Rogart, J. Nagata, C. S. Loeser, R. D. Roorda, H. Aslanian, M. E. Robert, W. R. Zipfel, and M. H. Nathanson, "Multiphoton imaging can be used for microscopic examination of intact human gastrointestinal mucosa ex vivo," Clin. Gastroenterol. Hepatol. **6**(1), 95–101 (2008).
24. L. Li, D. Kang, C. Feng, S. Zhuo, H. Tu, Y. Zhou, and J. Chen, "Label-free assessment of premalignant gastric lesions using multimodal nonlinear optical microscopy," IEEE J. Sel. Top. Quantum Electron. **25**(1), 1–6 (2019).
25. S. You, R. Barkalifa, E. J. Chaney, H. Tu, J. Park, J. E. Sorrells, Y. Sun, Y. Z. Liu, L. Yang, D. Z. Chen, M. Marjanovic, S. Sinha, and S. A. Boppart, "Label-free visualization and characterization of extracellular vesicles in breast cancer," Proc. Natl. Acad. Sci. U.S.A. **116**(48), 24012–24018 (2019).
26. W. Zheng, D. Li, and J. Y. Qu, "Monitoring changes of cellular metabolism and microviscosity in vitro based on time-resolved endogenous fluorescence and its anisotropy decay dynamics," J. Biomed. Opt. **15**(3), 037013 (2010).
27. J. W. Birk, M. Tadros, K. Moezardalan, O. Nadyarnykh, F. Forouhar, J. Anderson, and P. Campagnola, "Second harmonic generation imaging distinguishes both high-grade dysplasia and cancer from normal colonic mucosa," Dig. Dis. Sci. **59**(7), 1529–1534 (2014).
28. P. P. Provenzano, K. W. Eliceiri, J. M. Campbell, D. R. Inman, J. G. White, and P. J. Keely, "Collagen reorganization at the tumor-stromal interface facilitates local invasion," BMC Med. **4**(1), 38 (2006).
29. S Zhang, X. Huang, D. Kang, J. Miao, Z. Zhan, G. Guan, J. Chen, Y. Zhou, and L. Li, "Optical second-harmonic generation imaging for identifying gastrointestinal stromal tumors," J. Innov. Opt. Health Sci **2023**, 2350007 (2023).
30. L. Kreiß, O. M. Thoma, A. Dilipkumar, B. Carle, P. Longequeue, T. Kunert, T. Rath, K. Hildner, C. Neufert, M. Vieth, M. F. Neurath, O. Friedrich, S. Schurmann, and M. J. Waldner, "Label-free in vivo histopathology of experimental colitis via 3-channel multiphoton endomicroscopy," Gastroenterology **159**(3), 832–834 (2020).